CFD ANALYSIS OF SCREW COMPRESSOR PERFORMANCE

Ahmed Kovacevic, Nikola Stosic and Ian K. Smith

Centre for Positive Displacement Compressor Technology,
City University, London EC1V OHB, U.K.
e-mail: a.kovacevic@city.ac.uk

ABSTRACT

Modern manufacturing methods enable screw compressors to be constructed to such close tolerances that full 3-D numerical calculation of the heat and fluid flow through them is required to obtain the maximum possible improvements in their design. An independent stand-alone CAD-CFD interface program has therefore been developed by the authors in order to generate a numerical grid for this purpose. Modifications implemented to the CFD procedure improved solutions in complex domains with strong pressure gradients.

The interface employs a procedure to produce rotor profiles and an analytical transfinite interpolation method to obtain a fully structured 3-D numerical mesh, which is directly transferable to a CFD code. Some features, which include an adaptive meshing procedure, mesh orthogonalization and smoothing, are employed to generate a numerical mesh which can take advantage of the techniques used in recent finite volume numerical method solvers.

These were required to overcome problems associated with

i) rotor domains which stretch and slide relative to each other and along the housing
ii) robust calculations in domains with significantly different geometry ranges.
iii) a grid moving technique with a constant number of vertices.

Some changes had to be made within the solver functions to increase the speed of calculation. These include a means to maintain constant pressures at the inlet and outlet ports and consideration of two-phase flow resulting from oil injection in the working chamber.

The pre-processor code and calculating method have been tested on a commercial CFD solver to obtain flow simulations and integral parameter calculations.

The results of calculations on an oil injected screw compressor are presented in this paper and compared with experimental results.

LIST OF NOTATIONS

A - area of the cell surface
$\mathbf{a}_1$, $\mathbf{b}_1$ - radius vectors of boundary points
A_1, A_2 - saturation temperature equation constants
b_i - constant
B_1, B_2 - compressibility factor equation constants
c_i - concentration of species
c_1-c_4 - tension spline coefficients
C_1, C_2 - orthogonalization procedure coefficients
C_p - constant pressure specific heat
C, σ - constants in k-ε model of turbulence
d_i - distance in transformed coordinate system
d_o - Sauther mean diameter
D_1-D_4 - vapour specific heat equation constants
e_1, e_2 - cell edges maximal values in coordinate directions
$f^i(s)$ - adaptation variable
$\mathbf{f}_b$ - resultant body forces
$F^i(s)$ - integrated adaptation variable
h_1-h_8 - Hermite interpolation blending functions
h - enthalpy
h_L - enthalpy of vaporisation
k - turbulent kinetic energy
K_1, K_2 - coefficients for Hermite interpolation
m - mass
m_i - mass of species

Nu - Nuselt number
p - pressure
P - production of turbulence energy
Pr - Prandtl number
$\mathbf{q}_{ci}$ - diffusion flux of species
$\mathbf{q}_h$ - heat flux
$\mathbf{q}_k$ - diffusion flux in kinetic energy equation
$\mathbf{q}_\varepsilon$ - diffusion flux in dissipation equation
$\dot{Q}_{con}$ - convective heat flux
$\dot{Q}_{mass}$ - heat flux due to phase change
$\mathbf{r}$ - radius vector
Re - Reynolds number
R_i - grid point ratio
s - transformed coordinate
$\mathbf{s}$ - area vector
S_{ci} - source term of species
S_h - heat source term
$\mathbf{S}$ - viscous part of stress tensor
t - time
T - temperature
$\mathbf{T}$ - stress tensor
$\mathbf{v}$ - velocity
V - cell volume
w - weight factor
W - weight function
X_ξ - grid spacing
x, y, z - physical coordinates
X, Y, Z – points on physical boundaries
z - compressibility factor

α, β - tension spline coefficients
α_1, β_1 - blending functions
δ - Kroneker delta function
ε - dissipation of turbulent kinetic energy
κ - thermal conductivity
μ - viscosity
μ_t - turbulent viscosity
π - 3.14

ρ - density
σ - tension spline parameter
σ_{cv} - normalised cell volume
ξ, η - computational coordinates
$\hat{\xi}_o$, $\hat{\xi}_1$ - one-dimensional stretching functions
$\hat{\xi}$ - multi-dimensional stretching function

Indices:

add	- injected / subtracted fluid	*L*	- evaporated/condensed fluid
const	- constant prescribed value	*m*	- mixture
o	- oil	s	- grid values
v	- vapour	*sat*	- saturation
l	- liquid	*t*	- turbulence

1. INTRODUCTION

Approximately 17% of all electrical power generated is used to drive compressors while majority of such machines currently manufactured for industrial applications are of the screw type. Improvements in the efficiency of screw compressors can therefore lead to significant energy savings at global level.

Screw compressors are positive displacement rotary machines comprising a meshing pair of helical rotors on parallel axes, contained in a casing. Together, these form a succession of working chambers whose volume depends on the angle of rotation.

An outline of the main elements of a screw compressor is presented in Figure 1, which shows how the two rotors are contained in the casing. The main rotor, on the right, rotates counter clockwise, while the gate rotor, on the left, rotates clockwise. Admission of the gas to be compressed occurs through the low pressure port which is formed by opening of the casing surrounding the bottom and rear face of the rotors. Exposure of the space between the rotor lobes to the suction port, as their rear ends pass across it, allows the gas to fill the passage formed between them and the casing. Further rotation then leads to cut off of the port and progressive reduction in the trapped volume, thus causing the pressure of the contained gas to rise. The compression process continues until the front ends of the passages are exposed to the discharge port, the location of which is shown in outline. The gas flows out through this at approximately constant pressure.

Figure 1 Twin Screw Compressor Rotors and Casing Outline

The design parameter which influences screw compressor performance most strongly is the rotor profile and differences in shape, which can hardly be detected by the eye can effect significant changes in flow rates delivered and power consumption. Other features of the design also strongly affect the overall compressor performance. Thus, clearances between the rotors and between the rotors and the casing determine the leakage through the compressor and hence both the volume flow rate and the power consumption. The shape and position of the suction and discharge ports influence the dynamic losses and, in the case of oil injected machines, the oil injection port position and the quantity of oil injected into the working chamber affect both the outlet temperature and the power consumption. Dimensionless or quasi-steady mathematical models predict the overall effects of changes in these parameters on compressor overall behaviour fairly accurately. However, how the internal flow within the machine is affected locally by changes in these parameters is only approximated by such models. Consequently, the simplified analytical models currently in use are not sufficiently accurate to design screw compressors to obtain the maximum possible

improvements from the close manufacturing tolerances now achievable with contemporary numerically controlled machine tools.

It is therefore timely to apply a more complex analytical procedure, such as a 3-D Computational Fluid Dynamics (CFD) method to determine the effects of changes in the compressor geometry on internal heat and fluid flow. Such an approach can produce reliable predictions only if calculated over a substantial number of grid points. Hence, a high computer potential and capacity is needed in order to use such procedures to analyse a screw compressor. If an inadequate numerical grid is used, or the solver parameters are not selected carefully, a convergent numerical solution may not be obtained. Calculation results must therefore be monitored closely and compared with the experimental data in order to avoid obtaining results which do not accord with real flow conditions.

Apart from the authors' publications *[1]-[3]* and *[4]*, there is hardly any reported activity in the use of CFD for screw compressor studies. This is mainly because the existing grid generators and the majority of solvers are still too weak to cope with the problems associated with both the screw compressor geometry and physics of the compressor process. Since a screw compressor comprises both moving rotors and a stationary housing, any numerical grid applied must move, slide and deform. Moreover, if flow is to be calculated through the compressor clearances, the geometric length scale ratio of the working chamber may rise to 1000:1. Despite this, the grid aspect ratio should be kept very low. This cannot be done with the majority of existing CFD grid generators. Compressor flow, even in its simplest form, is further complicated by sharp pressure changes and high accelerations, which may drastically affect the flow structure. If, in addition, the working fluid is a real gas or a two-phase fluid or it contains particles, then there is hardly any CFD solver which can produce a straightforward solution. Therefore, special care is needed to blend the grid generation procedure with an adequate numerical solver to obtain a useful numerical solution of screw compressor processes.

Demirdzic and Peric, [5], [6] and *Peric [7]* set the guidelines for successful finite volume calculation of 3-D flows in complex curvilinear geometries. Based on this, *Ferziger and Peric [8]* published a book on finite volume methods for fluid dynamics. *Muzaferija [9]* applied unstructured grids and used a multigrid method to accelerate calculations. *Demirdzic and Muzaferija [10]* showed the possibility of simultaneous application of the same numerical methods in fluid flow and structural analysis within moving frames. Contemporary grid generation methods are extensively discussed by many authors. The most detailed textbooks are *Liseikin [11]* and *Thompson et al [12]*. Adequately applied, the grid generation they describe, accompanied by an appropriate CFD solver, can lead to the successful prediction of screw compressor thermo-fluid flow. Such an approach resulted in the algebraic grid generation method, which employs a multi parameter adaptation. This is given in detail by the authors in *[2] and [3]*, where an interface, which transfers the screw compressor geometry to a CFD solver, is also described and compressor suction flow is given as a working example.

An advanced grid generation procedure is described in this paper. By its use and the inclusion of additional source terms and boundary conditions in the standard governing equations, heat transfer and fluid flow within a screw compressor can be estimated by use of existing CFD solvers. Once the velocity and pressure distribution are determined within the compressor, overall performance parameters such as flow rate, rotor loads, torque and power input may be derived from them. Consequently, the more conventional performance criteria used by compressor manufacturers, such as specific power and volumetric and adiabatic efficiencies can be calculated. These derived values

may also be used for comparison of compressors and for further applications like rotor and compressor minimization and optimisation.

2 GENERATION OF A SCREW COMPRESSOR GRID

2.1 Fundamentals

An appropriate numerical grid must be generated as a necessary preliminary to a CFD calculation. The grid must define both the stationary and moving parts of the compressor. The rotors form the most complex part of the screw compressor grid and are the most important components since it is within the rotor interlobe chambers that the compression process occurs. Depending on the relative position of the rotors and the housing, the processes of suction, compression and discharge will occur within the compressor. Rotor rotation results in change in the volume of the chambers, which increases the pressure, while internal pressure changes cause leakage flow between the chambers.

To apply a CFD procedure, the compressor spatial domain is replaced by a grid which contains discrete volumes. The number of these volumes depends on the problem dimensionality and accuracy required. A composite grid, made of several structured grid blocks patched together and based on a single boundary fitted co-ordinate system is used to transform the compressor geometry into discrete volumes. Grids are then connected over defined regions on their boundaries which coincide with other parts of the entire numerical mesh. More details of the different grid types and the relative advantages of each grid system are given by *Shih et al [13]*.

The grid generation for compressor rotors starts with the definition of their spatial domains determined by the rotor profile coordinates and their derivatives. These are obtained by means of the rack generation procedure described in detail by *Stosic [14]*. The grid components define all connections between the rotors and the housing and contain the interlobe, tip and blow-hole leakage paths. The mesh calculation is based on an algebraic transfinite interpolation procedure with a static multi parameter adaptation. This includes stretching functions to ensure grid orthogonality and smoothness. More information about this particular grid generation method can be found in *[11]*. A grid for the stationary compressor components, like the housing and ports, is also produced. The suction port is divided into five sub-domains, while the discharge chamber consists of three sub-domains. The complete grid generation procedure is programmed in FORTRAN and ensures automatic grid formation for various compressor shapes and sizes, given the housing geometry parameters.

2.2 **Discretization of the screw compressor rotor boundaries**

In general, the number of points required to define the rotor geometry accurately is not large. However, the number needed to establish a sliding interface between them may be so large that the numerical mesh, so formed cannot be used. One means of resolving this problem, which combines accuracy with fast solution, is to keep the number of computational cells as low as possible and to modify the distribution of points according to local requirements. An additional reason for such an approach is the large aspect ratio of the screw compressor chamber, the dimensions of which vary from as little as 30 micrometers to tens of millimetres. In the case of the numerical mesh for the

compressor presented in this paper, the grid length scale ratio is approximately 500. Since the number of cells in the radial direction is the same in the chamber as in the gaps, the ratio between the circumferential and radial dimensions of the cell becomes unacceptable. However, the same number of cells can form a convenient grid if the boundary adaptation is applied carefully to keep the grid aspect ratio as uniform as possible.

In algebraic grid adaptation, most techniques are based on an equidistribution technique *[11]*. This is the technique where the distribution error is minimized by redistributing points along the curve to keep the product of a 'weight function' and the grid spacing constant, i.e.

$$X_x \, W = const. \tag{1}$$

where X_x represents grid spacing and W is a weight function. If the spacing of the computational coordinate is expressed with respect to the arc-length *s*, the adaptation function is in the form:

$$x(s) = \frac{\int_0^s W(s)ds}{\int_0^{S\max} W(s)ds}. \tag{2}$$

There are various approaches to define the weight functions. Samareh et al. *[16]* suggested the form:

$$W(s) = 1 + \sum_{i=1}^{I} b^i f^i(s), \tag{3}$$

where i is number of variables for adaptation, b^i are constants and $f^i(s)$ are adaptation variables or their first derivatives.

When the adaptation variables are integrated along the boundary curve and if the grid point ratio is R^i, the final form of the adaptation function becomes:

$$x(s) = \frac{s}{S_{\max}}\left\{1 - \sum_{i=1}^{I} R^i\right\} + \sum_{i=1}^{I}\left\{R^i \frac{F^i(s)}{F^i(S_{\max})}\right\}; \quad F^i(s) = \int_0^S f^i(s)ds \tag{4}$$

The majority of grid generation methods produce numerical grids by use of just one adaptation variable. However, within a complex geometry, various parameters determine the distribution of numerical points. For example, in the case of long narrow clearances, the distance between the points should be smaller. Similarly, a shorter distance between the points is needed in regions where the curvature is high. Also, the point distribution in the rotor contact area should be modified to fulfil the requirements of a block connection procedure in the CFD code. In such cases, adaptation by means of two or more variables or conditions is necessary. This is possible by use of an equidistance technique in the form of equation (4). The different adaptation criteria, like the radius of curvature, distance from the rotor centre or angle of the tangent are applied independently in the above mentioned boundary adaptation procedure, developed by the authors, to ensure a viable numerical grid. In the example given in the paper, two adaptation functions are used simultaneously. The tangent angle and a radius of curvature are applied to the male rotor. For the female rotor the flatness of the curve and the point centre distance are used as criteria for adaptation

2.3 **Transfinite interpolation**

To generate a three-dimensional numerical mesh of a screw compressor, the domain was divided into a number of cross sections along the rotor axis *Figure 5*. Each cross section was then calculated separately as a 2D face for both rotors by means of the following steps:

1) Transformation from the 'physical' domain to the numerical non-dimensional domain.
2) Definition of the edges by applying an adaptive technique,
3) Selection and matching of four non-contacting boundaries.
4) Calculation of the curves, which connect the facing boundaries by transfinite interpolation.
5) Application of a stretching function to obtain the distribution of the grid points.
6) Orthogonalization, smoothing and final checking of the grid consistency.

Once the boundary faces are produced in steps 1-3, the distribution of internal points in steps 4-6 can be found. A good summary of how to find the internal points from the boundary data by analytical transfinite interpolation is given by *Smith [17]*.
The coordinates of the two opposite boundaries expressed in vector form are:

$$\begin{aligned} \mathbf{a}_1(\xi,\eta) &= \mathbf{r}(\xi_l,\eta), \qquad l=1,2 \\ \mathbf{b}_1(\xi,\eta) &= \mathbf{r}(\xi,\eta_l), \qquad l=1,2\ , \end{aligned} \tag{5}$$

where the coordinates of the transformed computational coordinate system, ξ and η , are:

$$\xi = (i-1)/(I-1) \text{ and } \eta = (j-1)/(J-1)\ .$$

i and j denote point numbers on the physical coordinate while I and J are overall number of points on these coordinates. The interior point then can be calculated as:

$$\begin{aligned} \mathbf{r}_1(\xi,\eta) &= \sum_{l=1}^{2} a_1(\xi)\mathbf{a}_1(\eta) \\ \mathbf{r}\ (\xi,\eta) &= \mathbf{r}_1(\xi,\eta) + \sum_{l=1}^{2} b_1(\eta)[\mathbf{b}_1(\xi) - \mathbf{r}_1(\xi,\eta_l)]\ , \end{aligned} \tag{6}$$

The blending functions $a_1(\xi)$ and $b_1(\eta)$ can be arbitrary but must satisfy the cardinality conditions, given by (3), to ensure that the edges are reproduced as a part of the solution.

$$\begin{aligned} a_1(\xi_k) &= \delta_{kl}, \qquad k=1,2 \quad l=1,2 \\ b_1(\eta_k) &= \delta_{kl}, \qquad k=1,2 \quad l=1,2 \end{aligned} \tag{7}$$

δ is Kronecker's delta function *[11]*.

By use of equation (5), equation (6) for the 2-D domain can be written in the following general form, which connects the physical and numerical domain coordinates:

$$\begin{aligned} x(\xi,\eta) &= X_1(\xi,\eta)a_1(\xi) + X_2(\xi,\eta)a_2(\xi) \\ y(\xi,\eta) &= Y_1(\xi,\eta)\,b_1(\eta) + Y_2(\xi,\eta)\,b_2(\eta) \end{aligned} \tag{8}$$

The success of the analytical transfinite interpolation method (8) to produce regular distribution of the internal points is highly dependent on the selection of blending functions. The simplest method to obtain the blending functions is Lagrangian interpolation. However, it produces a satisfactory mesh only for simple problems and this is not case for the screw compressor.

A better and more accurate solution can be obtained by Hermite interpolation. More details of this are given by *Smith, [17]*, *Shih et al [13]*, and *Thomson et al [12]*. Only the final form of the equations is presented here. The four-boundary method, which assumes interpolation between all four boundaries of the 2-D domain can be written in the following form:

$$\begin{aligned} x(\boldsymbol{x},\boldsymbol{h}) &= x'(\boldsymbol{x},\boldsymbol{h}) + \Delta x(\boldsymbol{x},\boldsymbol{h}) \\ y(\boldsymbol{x},\boldsymbol{h}) &= y'(\boldsymbol{x},\boldsymbol{h}) + \Delta y(\boldsymbol{x},\boldsymbol{h}) \end{aligned} \tag{9}$$

If the second term in equation (9) is neglected, then the first term on the right hand side of the equation implements the two-boundary method, which interpolates between two non connecting boundaries:

$$\begin{aligned} x'(\boldsymbol{x},\boldsymbol{h}) &= X_1(\boldsymbol{x})h_1(\boldsymbol{h}) + X_2(\boldsymbol{x})h_2(\boldsymbol{h}) + \frac{\partial x(\boldsymbol{x},\boldsymbol{h}=0)}{\partial \boldsymbol{h}}h_3(\boldsymbol{h}) + \frac{\partial x(\boldsymbol{x},\boldsymbol{h}=1)}{\partial \boldsymbol{h}}h_4(\boldsymbol{h}) \\ y'(\boldsymbol{x},\boldsymbol{h}) &= Y_1(\boldsymbol{x})h_1(\boldsymbol{h}) + Y_2(\boldsymbol{x})h_2(\boldsymbol{h}) + \frac{\partial y(\boldsymbol{x},\boldsymbol{h}=0)}{\partial \boldsymbol{h}}h_3(\boldsymbol{h}) + \frac{\partial y(\boldsymbol{x},\boldsymbol{h}=1)}{\partial \boldsymbol{h}}h_4(\boldsymbol{h}) \end{aligned} \tag{10}$$

where h_1, h_2, h_3 and h_4 are the Hermite interpolation blending functions given as:

$$\begin{aligned} h_1 &= 2\boldsymbol{h}^3 - 3\boldsymbol{h}^2 + 1, & h_2 &= -2\boldsymbol{h}^3 + 3\boldsymbol{h}^2 \\ h_3 &= \boldsymbol{h}^3 - 2\boldsymbol{h}^2 + \boldsymbol{h}, & h_1 &= \boldsymbol{h}^3 - \boldsymbol{h}^2 \end{aligned} \tag{11}$$

The boundary points are defined as:

$$\begin{aligned} X_1 &= x(\boldsymbol{x},\boldsymbol{h}=0) = X_1(\boldsymbol{x}), & Y_1 &= y(\boldsymbol{x},\boldsymbol{h}=0) = Y_1(\boldsymbol{x}) \\ X_2 &= x(\boldsymbol{x},\boldsymbol{h}=1) = X_2(\boldsymbol{x}), & Y_2 &= y(\boldsymbol{x},\boldsymbol{h}=1) = Y_2(\boldsymbol{x}) \end{aligned} \tag{12}$$

The aim of the partial derivatives at the boundaries is to ensure orthogonality. These are:

$$\begin{aligned} \frac{\partial x(\boldsymbol{x},\boldsymbol{h}=0)}{\partial \boldsymbol{h}} &= K_1(\boldsymbol{x})\left(-\frac{\partial Y_1}{\partial \boldsymbol{x}}\right) & \frac{\partial x(\boldsymbol{x},\boldsymbol{h}=1)}{\partial \boldsymbol{h}} &= K_2(\boldsymbol{x})\left(-\frac{\partial Y_2}{\partial \boldsymbol{x}}\right) \\ \frac{\partial y(\boldsymbol{x},\boldsymbol{h}=0)}{\partial \boldsymbol{h}} &= -K_1(\boldsymbol{x})\left(-\frac{\partial X_1}{\partial \boldsymbol{x}}\right) & \frac{\partial y(\boldsymbol{x},\boldsymbol{h}=1)}{\partial \boldsymbol{h}} &= -K_2(\boldsymbol{x})\left(-\frac{\partial X_2}{\partial \boldsymbol{x}}\right) \end{aligned} \tag{13}$$

The coefficients K_1 and K_2 are positive numbers smaller than 1. They are usually chosen by trial and error to avoid the overlapping of connecting curves inside the domain.

For the four-boundaries method, only two additional boundaries have to be mapped. They are:

$$\begin{aligned} X_3 &= x(\boldsymbol{x}=0,\boldsymbol{h}) = X_3(\boldsymbol{h}), & Y_3 &= y(\boldsymbol{x}=0,\boldsymbol{h}) = Y_3(\boldsymbol{h}) \\ X_4 &= x(\boldsymbol{x}=1,\boldsymbol{h}) = X_4(\boldsymbol{h}), & Y_4 &= y(\boldsymbol{x}=1,\boldsymbol{h}) = Y_4(\boldsymbol{h}) \end{aligned} \tag{14}$$

If the second term in equation (9) is not neglected, it defines the mapping between the other two boundaries:

$$\Delta x(\boldsymbol{x},\boldsymbol{h}) = (X_3 - X'_3)h_5(\boldsymbol{x}) + (X_4 - X'_4)h_6(\boldsymbol{x}) + \left(\frac{\partial x(\boldsymbol{x}=0,\boldsymbol{h})}{\partial \boldsymbol{x}} - \frac{\partial x'(\boldsymbol{x}=0,\boldsymbol{h})}{\partial \boldsymbol{x}}\right)h_7(\boldsymbol{x}) + \left(\frac{\partial x(\boldsymbol{x}=1,\boldsymbol{h})}{\partial \boldsymbol{x}} - \frac{\partial x'(\boldsymbol{x}=1,\boldsymbol{h})}{\partial \boldsymbol{x}}\right)h_8(\boldsymbol{x})$$

$$\Delta y(\boldsymbol{x},\boldsymbol{h}) = (Y_3 - Y'_3)h_5(\boldsymbol{x}) + (Y_4 - Y'_4)h_6(\boldsymbol{x}) + \left(\frac{\partial y(\boldsymbol{x}=0,\boldsymbol{h})}{\partial \boldsymbol{x}} - \frac{\partial y'(\boldsymbol{x}=0,\boldsymbol{h})}{\partial \boldsymbol{x}}\right)h_7(\boldsymbol{x}) + \left(\frac{\partial y(\boldsymbol{x}=1,\boldsymbol{h})}{\partial \boldsymbol{x}} - \frac{\partial y'(\boldsymbol{x}=1,\boldsymbol{h})}{\partial \boldsymbol{x}}\right)h_8(\boldsymbol{x}) \quad (15)$$

The partial derivatives of the boundary points in the equation (15) are:

$$\begin{aligned}
\frac{\partial x'(\boldsymbol{x}=0,\boldsymbol{h})}{\partial \boldsymbol{x}} &= h_1(\boldsymbol{h})\frac{\partial x(\boldsymbol{x}=0,\boldsymbol{h}=0)}{\partial \boldsymbol{x}} + h_2(\boldsymbol{h})\frac{\partial x(\boldsymbol{x}=0,\boldsymbol{h}=1)}{\partial \boldsymbol{x}} \\
\frac{\partial x'(\boldsymbol{x}=1,\boldsymbol{h})}{\partial \boldsymbol{x}} &= h_1(\boldsymbol{h})\frac{\partial x(\boldsymbol{x}=1,\boldsymbol{h}=0)}{\partial \boldsymbol{x}} + h_2(\boldsymbol{h})\frac{\partial x(\boldsymbol{x}=1,\boldsymbol{h}=1)}{\partial \boldsymbol{x}} \\
\frac{\partial y'(\boldsymbol{x}=0,\boldsymbol{h})}{\partial \boldsymbol{x}} &= h_1(\boldsymbol{h})\frac{\partial y(\boldsymbol{x}=0,\boldsymbol{h}=0)}{\partial \boldsymbol{x}} + h_2(\boldsymbol{h})\frac{\partial y(\boldsymbol{x}=0,\boldsymbol{h}=1)}{\partial \boldsymbol{x}} \\
\frac{\partial y'(\boldsymbol{x}=1,\boldsymbol{h})}{\partial \boldsymbol{x}} &= h_1(\boldsymbol{h})\frac{\partial x(\boldsymbol{x}=1,\boldsymbol{h}=0)}{\partial \boldsymbol{x}} + h_2(\boldsymbol{h})\frac{\partial x(\boldsymbol{x}=1,\boldsymbol{h}=1)}{\partial \boldsymbol{x}}
\end{aligned} \quad (16)$$

while the remaining partial derivatives in the same equation are:

$$\begin{aligned}
\frac{\partial x(\boldsymbol{x}=0,\boldsymbol{h})}{\partial \boldsymbol{x}} &= -K_3(\boldsymbol{h})(-\frac{\partial Y_3}{\partial \boldsymbol{h}}) & \frac{\partial x(\boldsymbol{x}=1,\boldsymbol{h})}{\partial \boldsymbol{x}} &= -K_4(\boldsymbol{h})(-\frac{\partial Y_4}{\partial \boldsymbol{h}}) \\
\frac{\partial y(\boldsymbol{x}=0,\boldsymbol{h})}{\partial \boldsymbol{x}} &= K_3(\boldsymbol{h})(-\frac{\partial X_3}{\partial \boldsymbol{h}}) & \frac{\partial y(\boldsymbol{x}=1,\boldsymbol{h})}{\partial \boldsymbol{x}} &= K_4(\boldsymbol{h})(-\frac{\partial X_4}{\partial \boldsymbol{h}})
\end{aligned} \quad (17)$$

and the remaining Hermite factors are:

$$\begin{aligned}
h_5 &= 2\boldsymbol{x}^3 - 3\boldsymbol{x}^2 + 1, & h_6 &= -2\boldsymbol{x}^3 + 3\boldsymbol{x}^2 \\
h_7 &= \boldsymbol{x}^3 - 2\boldsymbol{x}^2 + \boldsymbol{x}, & h_8 &= \boldsymbol{x}^3 - \boldsymbol{x}^2
\end{aligned} \quad (18)$$

The four-boundary Hermite interpolation method gives a reasonably good distribution of internal points with the freedom to maintain the orthogonality and proper curvature on and near to the boundaries. However, this method sometimes causes the curves to overlap. This is a frequent case in complex domains, such as those of the screw compressor when the rotor interlobes have to match. If the overlapping problems cannot be overcome by this method, multidimensional stretching functions can be applied as proposed by *Steinthorrsson et al [18]*. These are calculated using Hermite interpolation and are given as:

$$\hat{\boldsymbol{x}}(\boldsymbol{x},\boldsymbol{h}) = \hat{\boldsymbol{x}}_0(\boldsymbol{x})h_1(\boldsymbol{h}) + \hat{\boldsymbol{x}}_1(\boldsymbol{x})h_2(\boldsymbol{h}) \quad (19)$$

h_1 and h_2 are the Hermite factors while $\hat{\boldsymbol{x}}_0(\boldsymbol{x})$ and $\hat{\boldsymbol{x}}_1(\boldsymbol{x})$ are one dimensional stretching functions where:

$$\hat{x}_0(x) = 0 \qquad for \quad i = 1$$
$$\hat{x}_0(x) = \frac{d_i}{d_L} \qquad for \quad i = 2,3,...L \tag{20}$$

and

$$d_i = \sum_{n=2}^{i} \sqrt{(x_n - x_{n-1})^2 + (y_n - y_{n-1})^2} \tag{21}$$

The problem associated with Hermite transfinite interpolation based on a cubic interpolation (11) and (18) is extensive skewness or overlap of the grid lines. Therefore, when the multidimensional stretching functions are employed for the Hermite interpolation, blending functions based on tension interpolation are used. The interpolation coefficients then become:

$$\begin{aligned}
h_1(s) &= c_1(1-s) + c_2 s + c_2\left[\frac{\sinh[(1-s)\sigma] - \sinh(s\sigma)}{\sinh(\sigma)}\right] \\
h_2(s) &= c_1 s + c_2(1-s) - c_2\left[\frac{\sinh[(1-s)\sigma] - \sinh(s\sigma)}{\sinh(\sigma)}\right] \\
h_3(s) &= c_3\left[(1-s) - \frac{\sinh[(1-s)\sigma]}{\sinh(\sigma)}\right] + c_4\left[s - \frac{\sinh(s\sigma)}{\sinh(\sigma)}\right] \\
h_4(s) &= -c_3\left[s - \frac{\sinh(s\sigma)}{\sinh(\sigma)}\right] - c_4\left[(1-s) - \frac{\sinh[(1-s)\sigma]}{\sinh(\sigma)}\right]
\end{aligned}, \tag{22}$$

with coefficients:

$$\begin{aligned}
c_1 &= 1 - c_2, & c_2 &= \frac{\sinh(\sigma)}{2\sinh(\sigma) - \sigma\ \cosh(\sigma) - \sigma} \\
c_3 &= \frac{-\alpha}{(\beta^2 - \alpha^2)}\sinh(\sigma), & c_4 &= \frac{\beta}{(\beta^2 - \alpha^2)}\sinh(\sigma) \\
\alpha &= \sigma\ \cosh(\sigma) - \sinh(\sigma), & \beta &= \sinh(\sigma) - \sigma
\end{aligned} \tag{23}$$

This method should generally be sufficient to produce a satisfactory grid for the CFD analysis of screw compressor flows. If this is not case, as for rotors with a very small radius on the lobe tip, orthogonalization and smoothing should be applied. The approach to the orthogonalization used for the screw compressor computational grid is similar to one suggested by *Lehtimaki, [11]*. After the regular, though not necessarily orthogonal and smooth mesh is produced by Hermite transfinite interpolation, additional orthogonalization and smoothing are applied. Mesh orthogonalization is achieved by moving the grid point perpendicularly to the normal to the boundary. A weighing factor between the original point $\mathbf{r}'_{i,j}$ and the orthogonal projection of this point to the line extending perpendicularly from the boundary $\mathbf{r}''_{i,j}$ is applied to avoid over specification caused by a discrepancy between the two boundaries. The coordinates of the new point are:

$$\mathbf{r}_{i,j} = (1 - w_{i,j})\mathbf{r}'_{i,j} + w_{i,j}\mathbf{r}''_{i,j} \tag{24}$$

The weighing factor has the exponential form:

$$w_{i,j} = \exp\left\{-C_1\left[\left(1 - \frac{\bar{\eta}_{i,j}}{\bar{\eta}_{i,j_{max}}}\right) - 1\right]\right\}\left[4\xi_{i,0}(1-\xi_{i,0})\right]^{C_2} \tag{25}$$

where $\hbar_{i,j} = \sqrt{(\chi_{i,j} - \chi_{i,0})^2 + (\eta_{i,j} - \eta_{i,0})^2}$. The coefficient C_1 in equation (25) controls the damping of the interior mesh. The second part of that equation is set to dump the end points of the boundary line where a high value of the coefficient C_2 implies that the grid has to be orthogonalized only in the central region of the boundary.

Smoothing of the interior lines is achieved by repetitive application of the following equations:

$$\begin{aligned} x_{i,j}^{n+1} &= x_{i,j}^{n} + C\left(x_{i+1,j}^{n} - 2x_{i,j}^{n} + x_{i-1,j}^{n}\right) \\ y_{i,j}^{n+1} &= y_{i,j}^{n} + C\left(y_{i+1,j}^{n} - 2y_{i,j}^{n} + y_{i-1,j}^{n}\right) \end{aligned} \tag{26}$$

where C is a constant and n=0,1,2…

Finally the grid must be checked for regularity. It can be accepted only if the skewness of all the cells within the domain is positive. This is calculated for every cell as a normalised cell volume $\sigma_{cv} = \dfrac{A}{e_1 e_2}$ where the area A is given as half of the cross product of the cell diagonals and e_1 an e_2 are maximal values of the cell edges in co-ordinate directions:

$$\begin{aligned} e_1 &= \max\left\{ \left|\vec{r}_{i+1,j} - \vec{r}_{i,j}\right|, \left|\vec{r}_{i+1,j+1} - \vec{r}_{i,j+1}\right| \right\} \\ e_2 &= \max\left\{ \left|\vec{r}_{i,j+1} - \vec{r}_{i,j}\right|, \left|\vec{r}_{i+1,j+1} - \vec{r}_{i+1,j}\right| \right\} \end{aligned} \tag{27}$$

Figure 2 Final numerical mesh for the screw compressor rotors in 2-D

The numerical mesh for the screw compressor rotors of 5/6 configuration produced by this complex method is shown in
Figure 2.

2.4 **CAD-CFD interface**

All the procedures described in the previous sections have been employed to form a stand alone CAD -CFD interface to generate a regular 3-D mesh of the screw compressor working volume. The interface program is written in Fortran and is called SCORG, **S**crew **C**Ompressor **R**otor **G**eometry grid generator. More information on the interface is given by *Kovacevic et al [1]*. The program calculates the meshing rotor coordinates from given rack or rotor curves, by means of two parameter adaptation, and then calculates the grids for both rotors. It also calculates the grids for the inlet and outlet ports and prepares the control parameters necessary for the CFD calculation of the compressor fluid flow.

A transfer file is given in ASCII format. This includes the node and cell definitions, regions, boundary conditions, control parameters and post-processing functions. The file can be imported into a commercial CFD package through its pre-processor. These should be able to process control volumes with an arbitrary number of faces. The solution domain can be split into several regions, with separate grid generation in each of them, without the need for grid matching at the region interfaces. Despite the non-matching interfaces, the discretization method is fully conservative and

all regions are coupled, so that the solution method converges as well as if the grid were made with one block only. This is very convenient when grids of different topology are generated to obtain the best fit for the geometry of each region. It is then possible to achieve high grid density without the large deformation that would result from a single-block grid. The grid may also be refined locally by subdividing selected cells into a number of smaller cells. The fact that the control volumes may have any number of faces and that the grids do not have to match at interfaces makes it possible to compute flows where the grid moves in some regions while it remains stationary in others.

2.5 **Grid for a 5/6 oil flooded compressor**

An oil-injected screw compressor, designed and built at City University, for which the flow field was calculated, is shown in *Figure 3*. The Rotor profiles are of the 'N' type *[14]* with a 5/6 lobe configuration. The rotor outer diameters are 128 and 101 mm for the male and female rotors respectively, and their centre lines are 90 mm apart. The rotor length to diameter ratio is 1.66. Both a drawing and a photograph of the rotors are presented in *Figure 4*.

Figure 3 Oil injected screw compressor with 'N' rotors.

The male and female rotors both have 40 numerical cells along one interlobe in the circumferential direction, 6 cells in the radial direction and 112 in the axial direction. This forms total number of 444830 cells for both the rotors and the housing. To avoid the need to increase the number of grid points if a more precise calculation is required, the adaptation method has been applied to the boundary definition.

Figure 4 Drawing and photograph of 5/6 male and female 'N' rotors

The compression in a screw compressor is caused by the rotor rotation induced by the driving motor coupled to the male rotor shaft. To simulate such a process, the numerical grid is modified for each time step. The number of time changes was 25 for one interlobe cycle, or 125 for the full rotation of the male rotor. The number of numerical cells on the rotors was kept the same for each time step. To achieve this, a special grid moving procedure was developed in which the time step was determined by the compressor speed. The numerical grid for the initial time step is presented in *Figure 5*.

Figure 5 Numerical grid for oil injected screw compressor with 444830 cells

3 CALCULATION PROCEDURE AND BOUNDARY CONDITIONS

3.1 Governing equations

Fluid compressed within a screw compressor is gas, vapour or a wet mixture of liquid and vapour and its density varies with both pressure and temperature. The compressor flow is fully described by the mass averaged equations of continuity, momentum and energy conservation, which are accompanied by the turbulence model equations and an equation of state, as given by the authors in *[3]*. Equations are given for the control volume V bounded by surface S in the integral form similar

for all conserved properties. They all contain local and convective rates of change on the left hand side and diffusive and source terms on the right hand side.

The continuity equation is:

$$\frac{d}{dt}\int_V \rho dV + \int_S \rho(\mathbf{v}-\mathbf{v}_s)\cdot d\mathbf{s} = 0, \tag{28}$$

where ρ is the density and **v** is the fluid velocity, while $\mathbf{v}_s$ is the grid velocity.

The momentum equation is:

$$\frac{d}{dt}\int_V \rho\mathbf{v} dV + \int_S \rho\mathbf{v}(\mathbf{v}-\mathbf{v}_s)\cdot d\mathbf{s} = \int_S \mathbf{T}\cdot d\mathbf{s} + \int_V \mathbf{f}_b dV, \tag{29}$$

where **T** is a stress tensor, and $\mathbf{f}_b$ is the resultant body force.

Since oil is injected into a screw compressor, the oil concentration $c_i = \frac{m_i}{m}$, where m is the overall mass, is calculated from its equation as a passive component, which affects the air in the source term of the mass and enthalpy equation. The concentration equation is:

$$\frac{d}{dt}\int_V \rho c_i dV + \int_S \rho c_i(\mathbf{v}-\mathbf{v}_s)\cdot d\mathbf{s} = \int_S \mathbf{q}_{ci}\cdot d\mathbf{s} + \int_V s_{ci} dV, \tag{30}$$

$\mathbf{q}_{ci}$ and s_{ci} denote the diffusion flux and source or sink of oil.
The transport equation of enthalpy is:

$$\begin{aligned}\frac{d}{dt}\int_V \rho h dV + \int_S \rho h(\mathbf{v}-\mathbf{v}_s)\cdot d\mathbf{s} = \int_S \mathbf{q}_h\cdot d\mathbf{s} + \int_V s_h dV + \\ \int_V \mathbf{S}:\nabla\mathbf{v}\, dV + \int_V \mathbf{v}\cdot\nabla p dV - \int_S p\mathbf{v}_s\cdot d\mathbf{s} + \frac{d}{dt}\int_V p dV\end{aligned} \tag{31}$$

where **S** is the viscous part of the stress tensor, p is pressure, $\mathbf{q}_h$ is the heat flux and s_h represents the heat source or sink.

Since screw compressor CFD calculations involve a moving grid, the equation of space conservation must be solved:

$$\frac{d}{dt}\int_V dV + \int_S \rho\mathbf{v}_s\cdot d\mathbf{s} = 0, \tag{32}$$

Stokes law is a constitutive relation that connects stress and rate of strain, through the viscosity m and complements the momentum equation, while the transport equations of concentration and enthalpy are closed by Fick's and Fourier's laws respectively.

Equations (28) to (32) are closed by the equation of state (33) and accompanied by equations of the k-ε turbulence model (34).

$$\rho = \rho(p,T) \tag{33}$$

$$\frac{d}{dt}\int_V \rho k dV + \int_S \rho k(\mathbf{v}-\mathbf{v}_s)\cdot d\mathbf{s} = \int_S \mathbf{q}_k \cdot d\mathbf{s} + \int_V (P-\rho\varepsilon)dV,$$
$$\frac{d}{dt}\int_V \rho\varepsilon dV + \int_S \rho\varepsilon(\mathbf{v}-\mathbf{v}_s)\cdot d\mathbf{s} = \int_S \mathbf{q}_\varepsilon \cdot d\mathbf{s} + \int_V (C_1 P\frac{\varepsilon}{k} - C_2\rho\frac{\varepsilon^2}{k} + C_3\rho\varepsilon\nabla\cdot\mathbf{v})dV \quad (34)$$

k and ε are the turbulent kinetic energy and its dissipation, $\mathbf{q}_k$ and $\mathbf{q}_\varepsilon$ are their diffusion fluxes, while P is the production of turbulence energy. $\mu_t = \rho C_m \frac{k^2}{\varepsilon}$ is the turbulent viscosity which complements viscosity μ. The constants of the k-ε turbulence model are: C_m =0.09, σ_k =1, σ_ε =1.3, C_1=1.44, C_2 =1.92, C_3= -0.33. Standard wall functions are implemented on the walls

3.2 Specific aspects of the compressor CFD calculation

3.2.1 Oil injection and two phase flow

It is a common situation to have multiphase flow in the screw compressor. When the working media is a two-phase fluid, as for example in refrigeration compressors, a two-phase flow occurs. In such a situation a part of the fluid may evaporate or condense. The liquid phase of the working fluid is then treated as an 'active' phase, which requires all governing equations to be solved for the vapour – liquid mixture. The thermodynamic state of the mixture has a significant influence on the energy equation through the evaporated or condensed mass and the accompanying enthalpy of vaporisation. On the other hand, in the case of oil-flooded screw compressors the oil injected into the working chamber is treated as a dispersed phase and considered through its concentration. The oil fulfils several duties in the oil injected screw compressor since it seals, lubricates and cools the compressor working chamber. The influence of oil on the background fluid is accounted for by the convective heat flux, which is contained in the energy equation. However, the oil is treated as a 'passive' species.

The energy balance for two-phase flow with oil injection is given in the following form:

$$C_p \frac{d(mT)}{dt} = \dot{Q}_{con} + \dot{Q}_{mass}, \quad (35)$$

The convective heat flux between the air and oil is given by:

$$\dot{Q}_{con} = m_o C_{p_o} \frac{dT}{dt} = \pi d_o \kappa Nu\,(T - T_o), \quad (36)$$

and the heat flux caused by mass transfer between the phases is:

$$\dot{Q}_{mass} = \frac{dm_L}{dt} h_L. \quad (37)$$

where h_L is the enthalpy of vaporisation. Energy exchanged during the evaporation or condensation processes should be the same as the energy required to keep the temperature of the mixture at its saturated value corresponding to the pressure within the control volume, ie:

$$\dot{Q}_{mass} = \Delta m_L \cdot h_L = m \cdot C_{pm} \cdot (T - T_{sat}) \quad (38)$$

where m is the mass of mixture, C_{pm} is the constant pressure specific heat of the mixture of liquid and vapour and T_{sat} is the saturated vapour temperature. The calculating procedure for these values is presented in section 3.2.2.

In these equations C_{po}, T_o and $\boldsymbol{k}$ are the specific heat, temperature and the thermal conductivity of oil, while Nu is the Nusselt number. The Sauter mean diameter d_o is the parameter, which through adequate area determines heat transfer between the dispersed and continuous phase. For the ordinary oil injected screw compressor, its value is usually between 10 and 50 μm. *Stosic at al* gave more details on this in *[19]*.

3.2.2 Equation of state for real fluids

Screw compressors often work with fluids that cannot be regarded as ideal. This is the common situation in refrigeration and air conditioning systems. If the flow of the real fluid has to be solved, the following thermodynamic parameters are required: saturation temperature, density of the mixture, its specific heat, enthalpy of vaporization and the constant $C_{\boldsymbol{r}}$. The latest one appears in the correction for mass flux in the coupling of the mass flow equation and the equation of state, as presented by *Ferziger and Peric [8]*.

There are standard software packages available for calculation of real fluid properties, like NIST and IIR routines. However, the variables derived from them are expressed implicitly and therefore are obtained by iterative procedures which are too slow for CFD calculations. Therefore, to accelerate the calculation, a simple explicit equation of state is used employing a compressibility factor *z*:

$$\frac{p}{\boldsymbol{r}_v} = z \cdot RT \tag{39}$$

where $\boldsymbol{r}_v$ is the vapour density at the given pressure and temperature. The compressibility factor is assumed as linear function of pressure:

$$z = B_1 p + B_2, \tag{40}$$

where B_1 and B_2 are constants different for each fluid. If the fluid is ideal B_1=0 and B_2=1. Otherwise B_1 is usually negative and B_2 is less then 1. The coefficients B_1 and B_2 are calculated from known thermodynamic properties at saturated conditions for pressures between 1 and 20 bar. Screw machines usually operate within that range of working pressures regardless the application and the approximation does not introduce more than 2 % error into calculation of thermodynamic properties. The density of the liquid phase is assumed constant and the density of the mixture is thereby calculated as:

$$\boldsymbol{r} = \frac{1}{\dfrac{1-c_l}{\boldsymbol{r}_v} - \dfrac{c_l}{\boldsymbol{r}_l}} \tag{41}$$

where c_l is the concentration of the liquid phase in the control volume.

Saturation temperature is calculated from the modified Antoine equation in the form which gives saturation temperature explicitly for a known pressure:

$$T_{sat} = \frac{A_2}{A_1 - \log p} \tag{42}$$

where A_1 and A_2 are constants. The enthalpy of vaporisation is calculated at the working saturation pressure by means of the Clausius-Clapeyron equation which may be written as:

$$h_L = T_{sat}\, v_{lv} \left(\frac{dp}{dT} \right)_{sat}, \tag{43}$$

where v_{lv} is the difference between the vapour and liquid specific volumes.

The specific heat of the mixture C_{pm} is the mass weighted sum of the vapour and liquid specific heats, C_{pv} and C_{pl}. The specific heat of the liquid is assumed to be constant, while the specific heat of the vapor is expressed as a cubic polynomial:

$$C_{pv} = D_0 + D_1 T + D_2 T^2 + D_3 T^3 \tag{44}$$

where D_0, D_1, D_2 and D_3 are constants different for each fluid.

3.2.3 Boundary conditions

A special treatment of the compressor boundaries was introduced in the numerical calculation as follows. The compressor was positioned between relatively small suction and discharge receivers. Therefore, the compressor system was separated from its surroundings only by walls. It communicates with the surroundings through the mass and energy source or sink placed in these receivers to maintain constant suction and discharge pressures. A volume source is used in the pressure correction procedure as the amount of mass added or removed from the computational cell within the receivers. It is calculated from the difference between the calculated pressure p and required pressure p_{const} as:

$$\dot{m}_{add} = \left(\frac{dm}{dt} \right)_{p=const} \approx \frac{p_{const} - p}{p_{const}} \frac{V\, \rho}{\Delta t} \tag{45}$$

where V is the cell volume and ρ is the density. The volume source for the receiver cells in the energy equation is calculated from that mass as:

$$\dot{Q}_{add} = h_{add} \left(\frac{dm}{dt} \right)_{p=const} = \dot{m}_{add}\, h_{add} \tag{46}$$

The compressor intake and discharge flows and pressure change within the compressor are solely due to the rotor movement. This allows the compressor calculation to start from rest with relatively coarse initial conditions and establish a full solution after only a fraction of a compressor cycle. Such an approach is different from the standard inlet and outlet boundary conditions, or pressure boundary condition. The first would not allow a flow reversal at the compressor discharge, while the latter would be prohibitively slow due to the unsteady character of the compressor process. This novel approach therefore introduces additional stability to accelerate calculation. The procedure secures full and precise control of the pressures in both reservoirs and reduces the calculation time required by a factor of five compared with any other approach. The same was used for the boundary conditions in the oil injection port.

3.3 Calculation of the compressor performance

Once the velocity, temperature and pressure fields in the compressor are calculated, the compressor volume flow is obtained at the screw compressor suction as a scalar product of the fluid velocity and corresponding surface vectors for each cell. When multiplied by the corresponding density and integrated over the entire cross section, compressor volume flow gives the compressor mass flow. Finally, the volume and mass flows were averaged for all time steps. A similar procedure was applied to calculate the outlet mass flow. Mass flow of the oil through the oil injection port was calculated from the mass concentration of oil in its port. The inlet air and oil injected mass flows should be equal to the outlet mass flow of the mixture for steady working conditions.

Since the pressure in the working chamber does not vary too much in one interlobe within one time step, it was sufficiently accurate to average the pressure values arithmetically in each working chamber to plot pressure-shaft angle, p-α diagrams for all interlobes in all the time steps of the working cycle.

However, the calculation of the torque and forces acting on the rotors requires pressure values in each cell of the working chamber to be considered. The forces acting on the rotor, which are caused by pressure in the working chamber, are calculated as a product of the pressure at the rotor face cell boundary and the corresponding cell area vector. The resultant force has three components, one in the rotor axial and two in the transverse directions. The cross product of the force and its coordinate forms a force moment, the components of which act in three directions. Two of them serve to calculate axial and radial force reactions in the suction and discharge bearings, while the third component is the torque acting on both, the male and female rotors. To obtain integral radial and axial forces and torque, the cell values are summed over the entire surfaces of both rotors.

Once obtained, the torque is used to calculate the compressor power transmitted to the rotor shaft as a product of the torque and shaft speed. The shaft power should correspond to the indicated power calculated from the p-V diagram. Compressor specific power is calculated as the ratio of the input power to the compressor volume flow. The volumetric efficiency is calculated as the ratio of the compressor volume flow to the compressor theoretical displacement and the compressor adiabatic efficiency is calculated as the ratio of the compressor theoretical adiabatic power: to either the shaft or indicated power.

4 RESULTS AND DISCUSSION

4.1 Compressor measurements

In the absence of flow field measurements in the compressor chamber, the experimentally obtained pressure history within the compressor cycle and the measured air flow and compressor power served as a valuable basis to validate the results of the CFD calculation. To obtain these values, the 5/6 oil flooded compressor, already described, was tested on a rig built at City University, which has been certified by Lloyd's of London as fully meeting Pneurop/Cagi requirements for screw compressor acceptance tests. The compressor was tested according to the procedures specified in

ISO 1706 and the delivered flow was measured in accordance with BS 5600. High accuracy test equipment was used for the measurement of all relevant parameters.

All measurements were made by transducers and both recorded and processed in a computerized data logger for real time presentation. A screen record of the compressor measurement is given in *Figure 6*. A Diesel engine of 100 kW maximum power output, which can operate at variable speed, was used as the prime mover. This permits the testing of oil-flooded screw compressors with discharge rates of up to 16 m^3 /min.

Figure 6 Compressor test layout and the computer screen

4.2 CFD calculation

A numerical solution of the system of equations was obtained from the CFD solver 'Comet', which is developed by the Institute of Computational Continuum Mechanics GmbH. This code is applicable not only to fluid flow but also for solid body analysis. It also meets the needs of coupled computation of gas and liquid flow including moving surfaces, non-Newtonian fluids, flows with both highly compressible as well as incompressible regions, flows with moving boundaries and particle flows. Hence, it contains all the essential features needed to obtain the ultimate aims of full machine simulation. All additional terms described in previous chapter were introduced through user functions. The numerical mesh produced by the stand-alone grid generator was automatically transferred to the CFD solver together with all control parameters and user functions.

To establish a full range of working conditions and to obtain an increase of pressure from 1 to 5, 7 or 9 bars between the compressor suction and discharge with a numerical mesh of nearly 450000 cells, only 25 time steps were required, following which a further 25 time steps were needed to complete a full compressor cycle. Each time step needed about 30 minutes running time on an 800 MHz AMD Athlon processor. The computer memory required was about 450 MB.

4.3 Comparison of the CFD results and experimental data

Results of the CFD calculation of an oil injected air compressor are presented in *Figure 7-Figure 10*. Variation of pressure within the working cycle calculated from the CFD estimate is compared with measured values in *Figure 11*. The forces acting on the rotors and the bearing forces are shown in *Figure 12* and *Figure 13*.

In *Figure 7* and
Figure 8 the velocity vectors in two cross sections and two different time steps in the axial section are compared respectively. The high values of velocity in gaps both between the rotors and their housing and between the two rotors generated by the sharp pressure gradient through the clearances are clearly distinguished from the velocities in the highly turbulent regions in the interlobes where the movement is relatively slower. Velocity changes in space and time, as presented in two cross sections in the *Figure 7*, are caused only by the movement of the numerical mesh, which follows the rotation of the rotors. Velocity field in the axial section is shown in
Figure 8.

Figure 7 Velocity vectors in the two compressor cross sections

Left – suction port, Right – working chamber

Figure 8 Velocity vectors in the compressor axial section

Figure 9 Cross section through the inlet port and oil injection port

(Left – mass concentration of oil, Right - Pressure distribution)

Figure 10 Axial section between two rotors

(Top – mass concentration of oil, Bottom - Pressure distribution)

The oil and pressure distribution in the cross section with the oil injection port are shown in *Figure 9*. The pressure rise within the machine when rotating at 5000 rpm with a discharge pressure of 7 bar absolute is shown in *Figure 10*. The estimated thermodynamic and flow properties presented in previous figures were later used for calculation of the overall parameters of the analysed screw compressor.

Figure 11 Pressure-shaft angle diagram, comparison of CFD calculations and measurements

Figure 12 Radial bearing forces acting on supporting bearings compared for CFD and one-dimensional model

The pressure within the working chamber is shown in *Figure 11*, where pressure-shaft angle diagrams are presented and compared with the results obtained with measurements on the modelled screw compressor. The given results were obtained for a shaft speed of 5000 rpm and discharge pressures of 6, 7, 8 and 9 bar absolute. In all cases, the inlet pressure was 1 bar. The agreement between the predicted and estimated values is highly encouraging.

Figure 13 Torque on the male and female rotors

The radial bearing forces are given in *Figure 12*, while the torque on the male and female rotors are given in *Figure 13*.

The compressor delivery and power of both CFD calculations and measurements for three different discharge pressures are presented in *Figure 14*.

Figure 14 Comparison of the integral parameters at 5000 rpm shaft speed

5 CONCLUSION

Full CFD solutions of compressor thermodynamics and fluid flow have been obtained for an oil injected air compressor and integral compressor parameters such as the compressor flow, power, specific power and volumetric and adiabatic efficiencies have been derived from them. The

compressor performance for two different discharge pressures obtained with a CFD model based on the **SCORG, S**crew **CO**mpressor **R**otor **G**eometry grid generator, and calculated by a commercial CFD solver **COMET**, have been compared with test results obtained from a real compressor. The good agreement between predicted and measured performance is a strong indication that CFD analysis can be developed further as a powerful tool for the design and optimisation of screw compressors.

REFERENCES

1. **Kovacevic A, Stosic N, Smith I. K.** Development of CAD-CFD Interface for Screw Compressor Design, *International Conference on Compressors and Their Systems, London, IMechE Proceedings, 1999,757*
2. **Kovacevic A, Stosic N, Smith I. K.** The CFD Analysis of a Screw Compressor Suction, *International Compressor Engineering Conference at Purdue, 2000, 909*
3. **Kovacevic A, Stosic N, Smith I. K.** Grid Aspects of Screw Compressor Flow Calculations, *Proceedings of the ASME Congress- 2000, Advanced Energy Systems Division, 2000, Vol. 40, 83*
4. **Stosic N, Smith I. K, Zagorac S.** CFD Studies of Flow in Screw and Scroll Compressors, *XIII Int. Conf on Compressor Engineering at Purdue 1996*
5. **Demirdzic I, Peric M.** Finite Volume Method for Prediction of Fluid flow in Arbitrary Shaped Domains with Moving Boundaries, *Int. J. Numerical Methods in Fluids, 1990, Vol. 10, 771*
6. **Demirdzic I, Lilek Z, Peric, M.** A Collocated Finite Volume Method for Predicting Flows at All Speeds, *Int. J Numerical Methods in Fluids, 1993, Vol. 16, 1029*
7. **Peric, M.** A Finite Volume Method for the Prediction of Three Dimensional Fluid Flow in Complex Ducts, *PhD Thesis, Imperial College of Science, Technology & Medicine, London, 1985*
8. **Ferziger J H, Peric, M.** *Computational Methods for Fluid Dynamics, Springer, Berlin, Germany, 1996*
9. **Muzaferija S.** Adaptive Finite Volume Method for Flow Prediction Using Unstructured Meshes and Multigrid Approach, *PhD Thesis, Imperial College of Science, Technology & Medicine, London, 1994*
10. **Demirdzic I, Muzaferija S.** Numerical Method for Coupled Fluid Flow, Heat Transfer and Stress Analysis Using Unstructured Moving Mesh with Cells of Arbitrary Topology, *Comp. Methods Appl. Mech Eng, 1995, Vol. 125, 235-255*
11. **Liseikin V.D.** Grid generation Methods, *Springer-Verlag, 1999*
12. **Thompson J.F, Soni B, Weatherrill N.P.** Handbook of Grid generation, *CRC Press 1999*
13. **Shih T. I. P, Bailey R. T, Ngoyen H.L, Roelke R.J.** Algebraic Grid Generation For Complex Geometries, *International Journal for Numerical Methods in Fluids, 1991, Vol. 13, 1-31*
14. **Stosic N,** On Gearing of Helical Screw Compressor Rotors, *Proc IMechE, Journal of Mechanical Engineering Science, 1998, Vol.212, 587*
15. **Lehtimaki R.** An Algebraic Boundary Orthogonalization Procedure for Structured Grids, *International Journal for Numerical Methods in Fluids, 2000,Vol. 32, 605-618*
16. **Samareh-Abolhassani J, Smith R.E.** A Practical Approach to Algebraic Grid Adaptation, *Computers Mathematical Applications, 1992, Vol.24, No.5/6, 69-81*
17. **Smith R.E.** Algebraic Grid Generation, from Numerical Grid Generation, ed. By Thomson J.FG, *Elsevier Publishing Co, 1982, 137*
18. **Steinthorsson E, Shih T. I. P, Roelke R. J.** Enhancing Control of Grid Distribution In Algebraic Grid Generation, *International Journal for Numerical Methods in Fluids, 1992, Vol. 15, 297-311*
19. **Stosic N, Milutinovic Lj, Hanjalic K, Kovacevic A.** Investigation of the Influence of Oil Injection upon the Screw Compressor Working Process, *Int.J.Refrig. 1992, 15,4,206*

LIST OF CAPTIONS

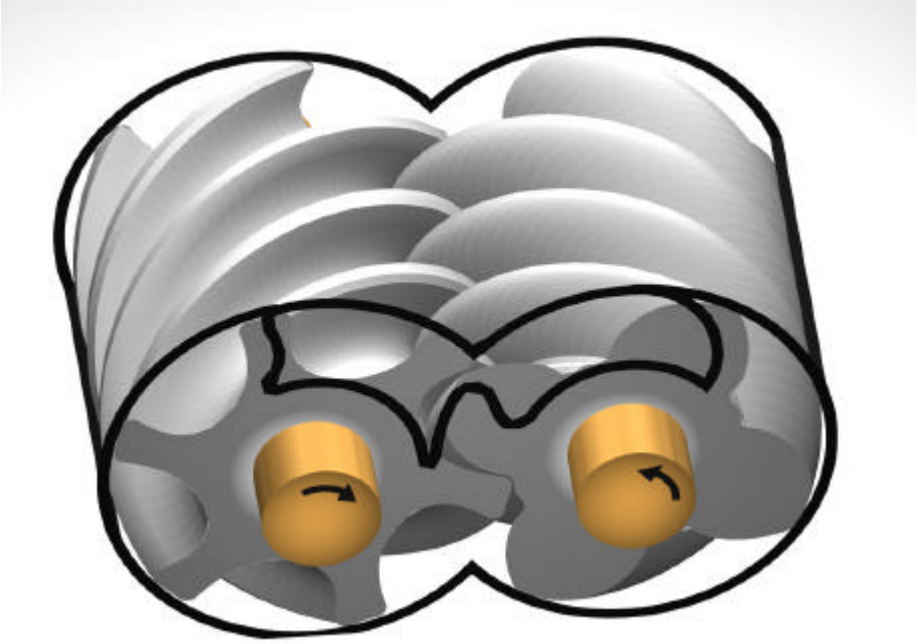

Figure 1 Twin Screw Compressor Rotors and Casing Outline

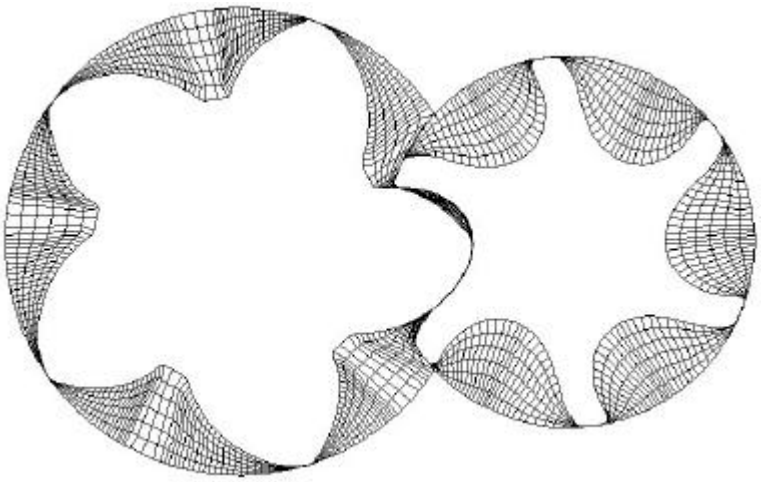

Figure 2 Final numerical mesh for the screw compressor rotors in 2-D

Figure 3 Oil injected screw compressor with 'N' rotors.

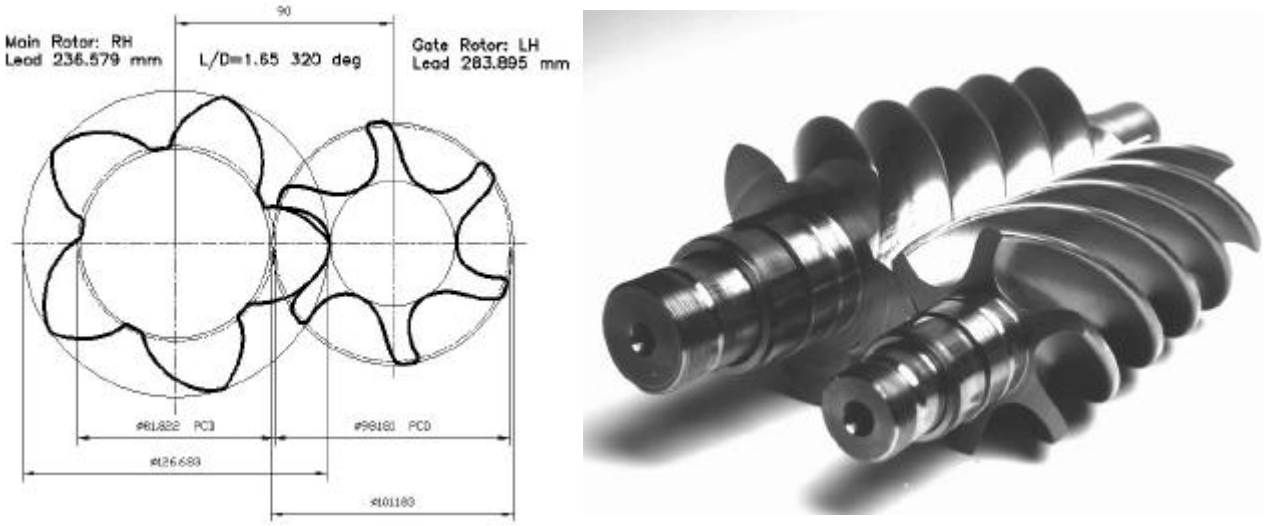

Figure 4 Drawing and photograph of 5/6 male and female 'N' rotors

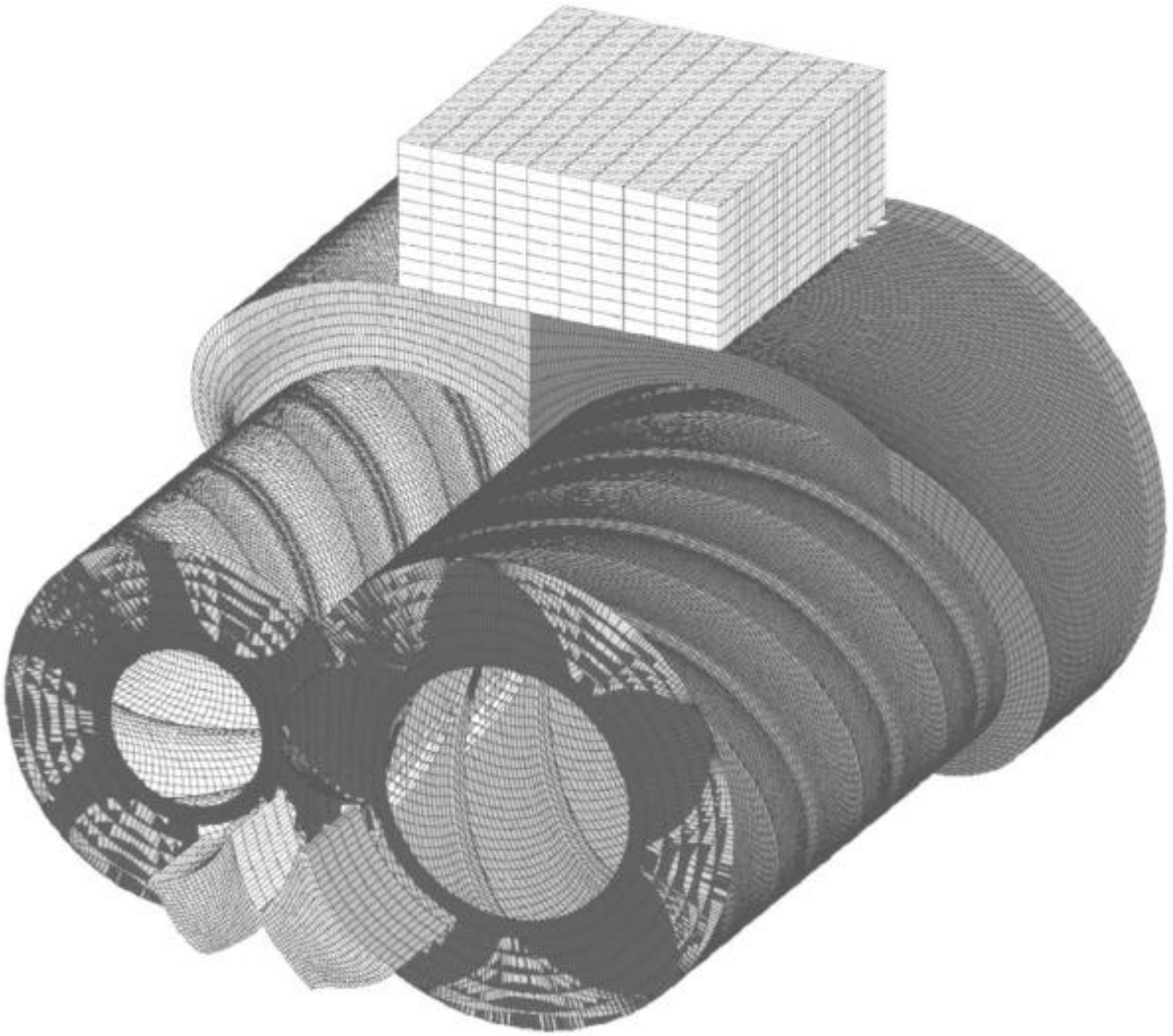

Figure 5 Numerical grid for oil injected screw compressor with 444830 cells

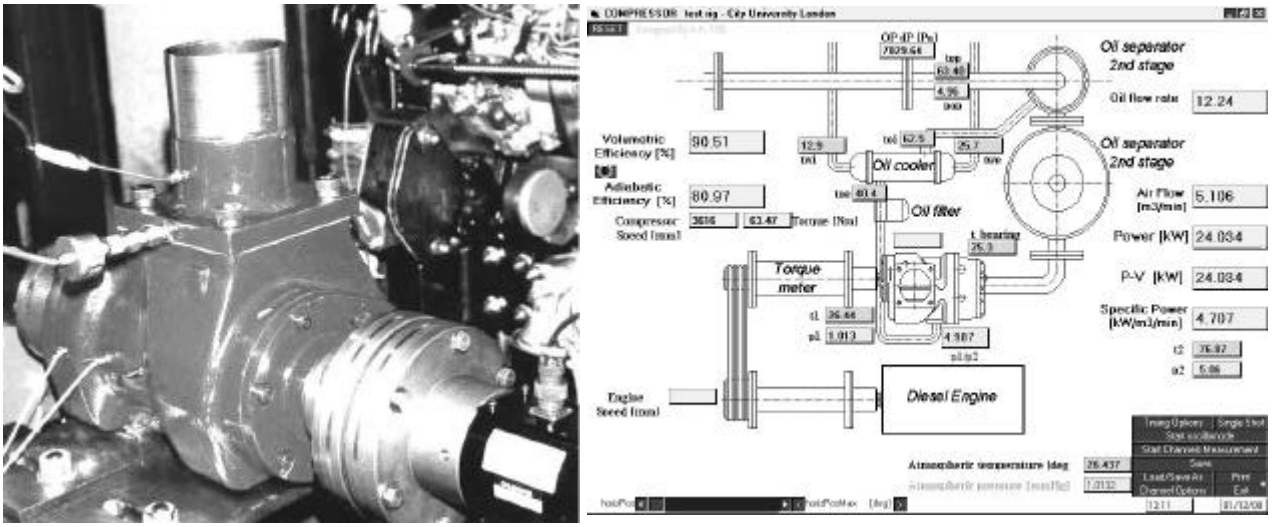

Figure 6 Compressor test layout and the computer screen

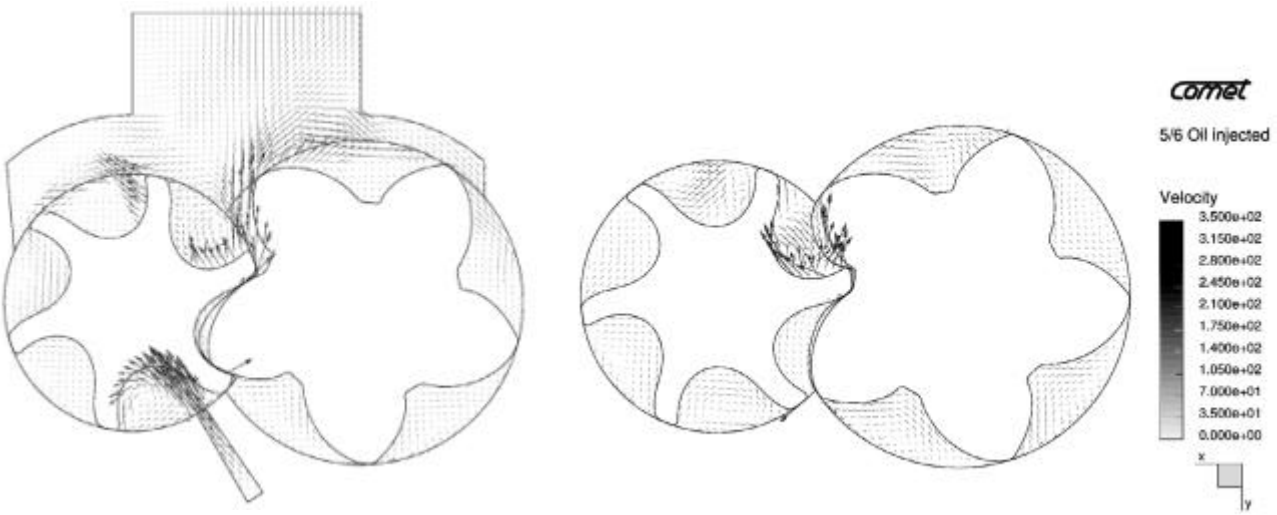

Figure 7 Velocity vectors in the two compressor cross sections

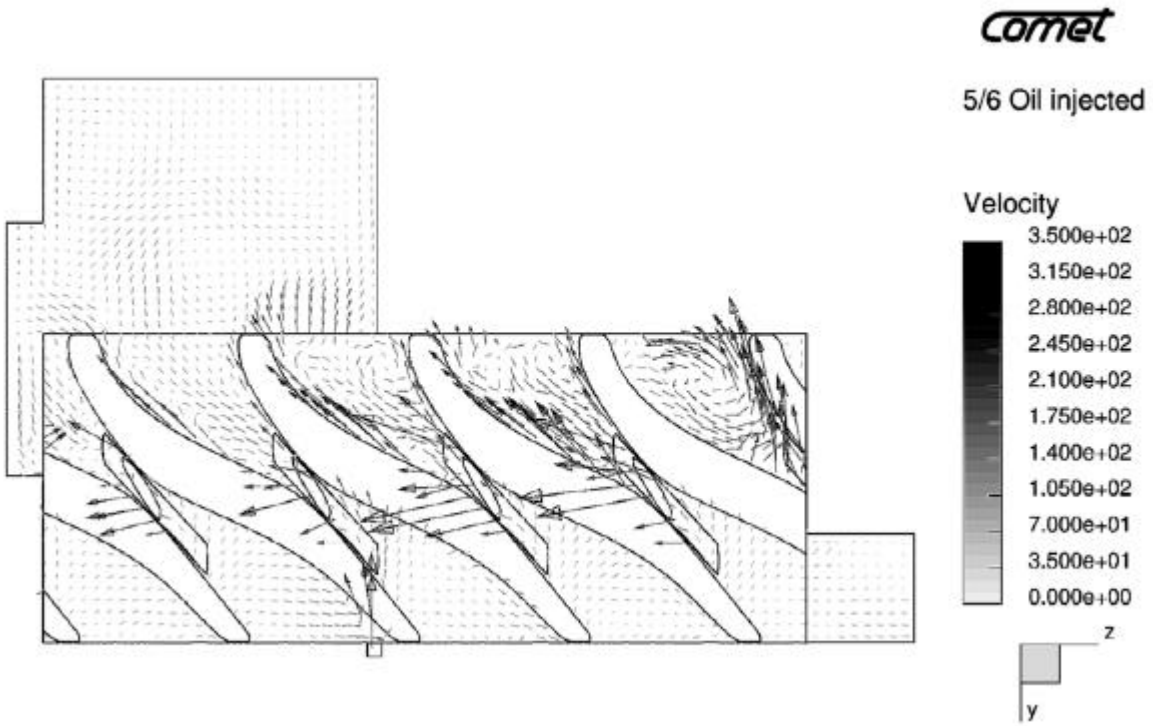

Figure 8 Velocity vectors in the compressor axial section

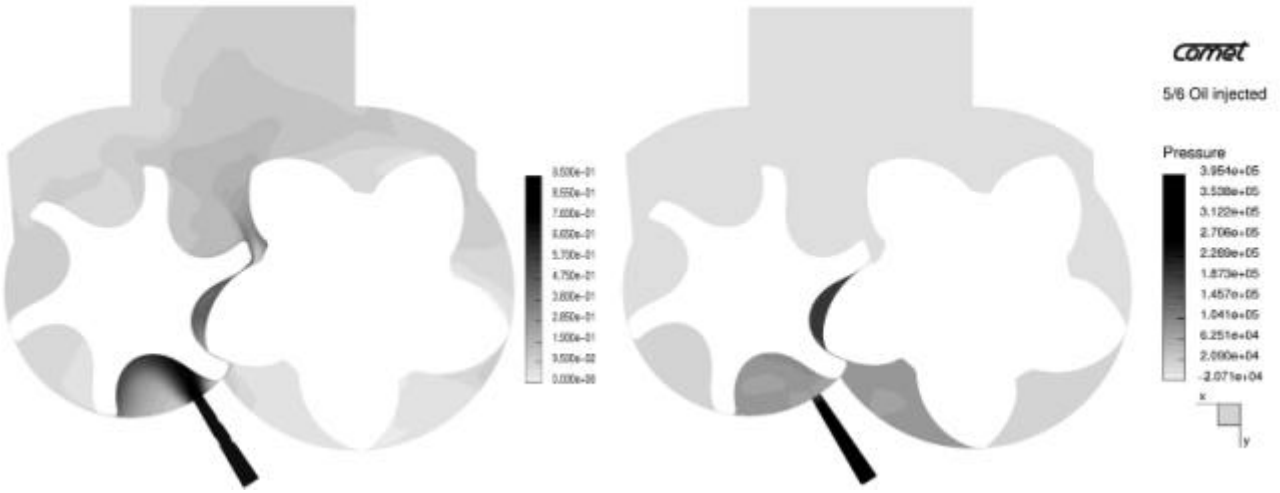

Figure 9 Cross section through the inlet port and oil injection port

Figure 10 Axial section between two rotors

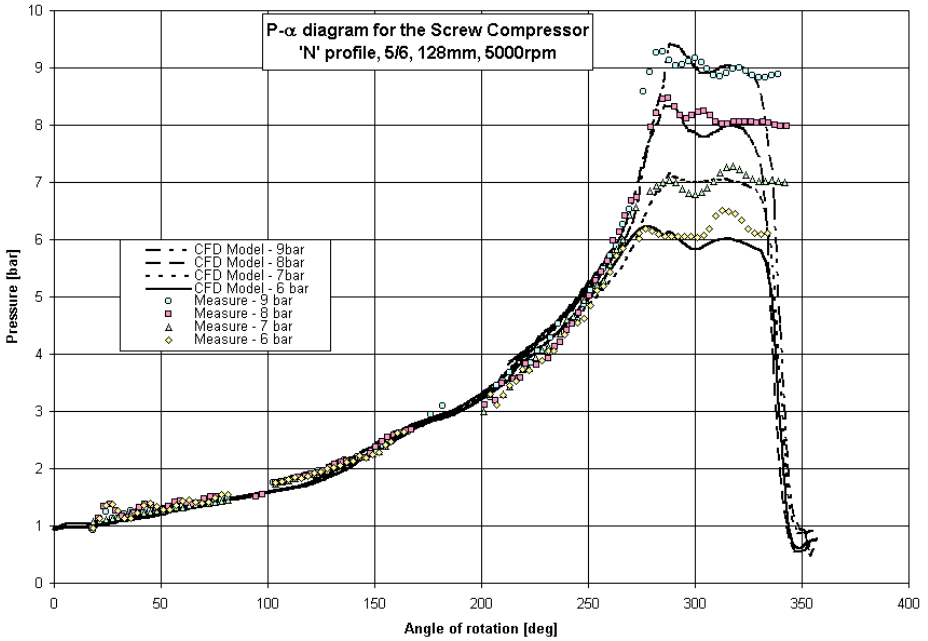

Figure 11 Pressure-shaft angle diagram, comparison of CFD calculations and measurements

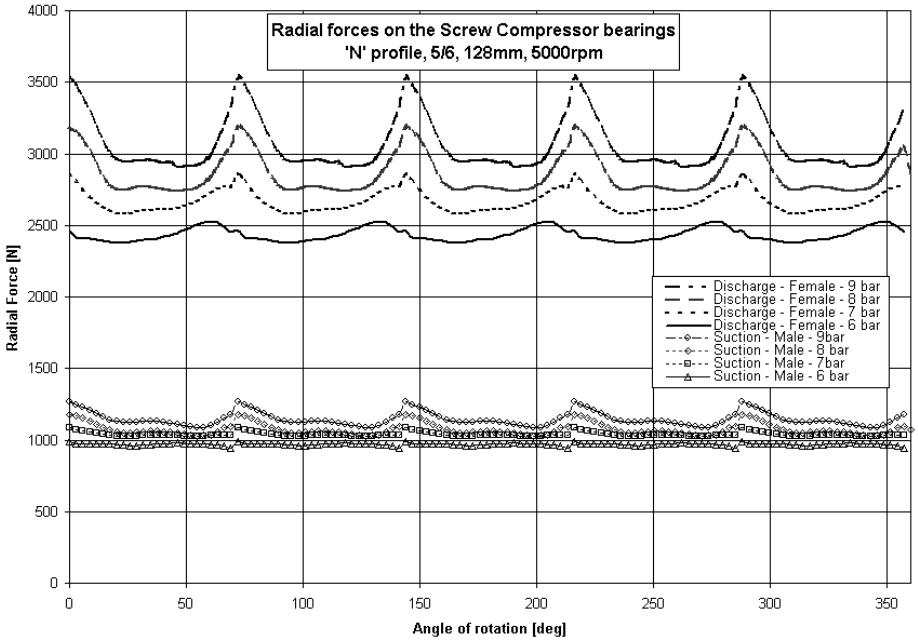

Figure 12 Radial bearing forces acting on supporting bearings compared for CFD and one-dimensional model

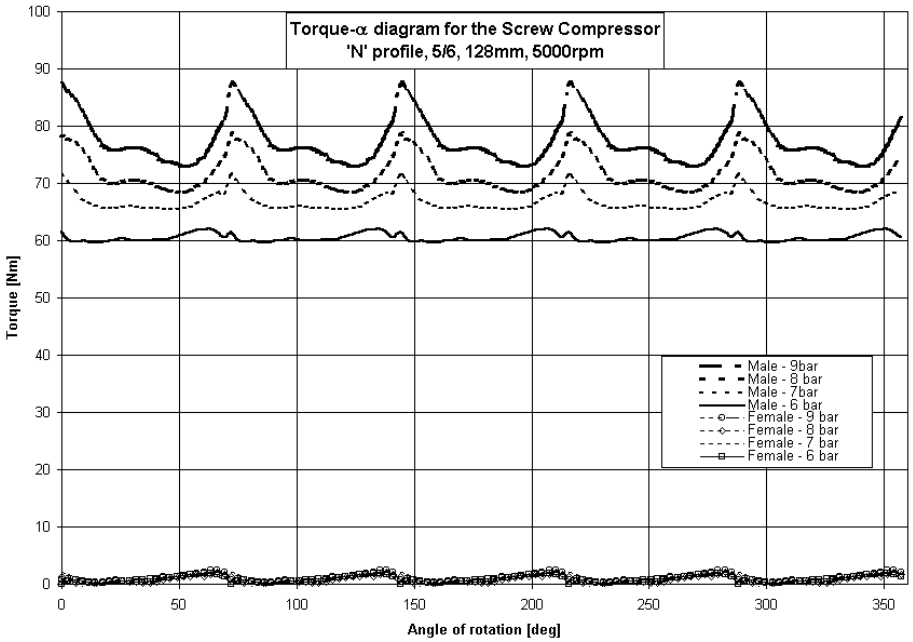

Figure 13 Torque on the male and female rotors

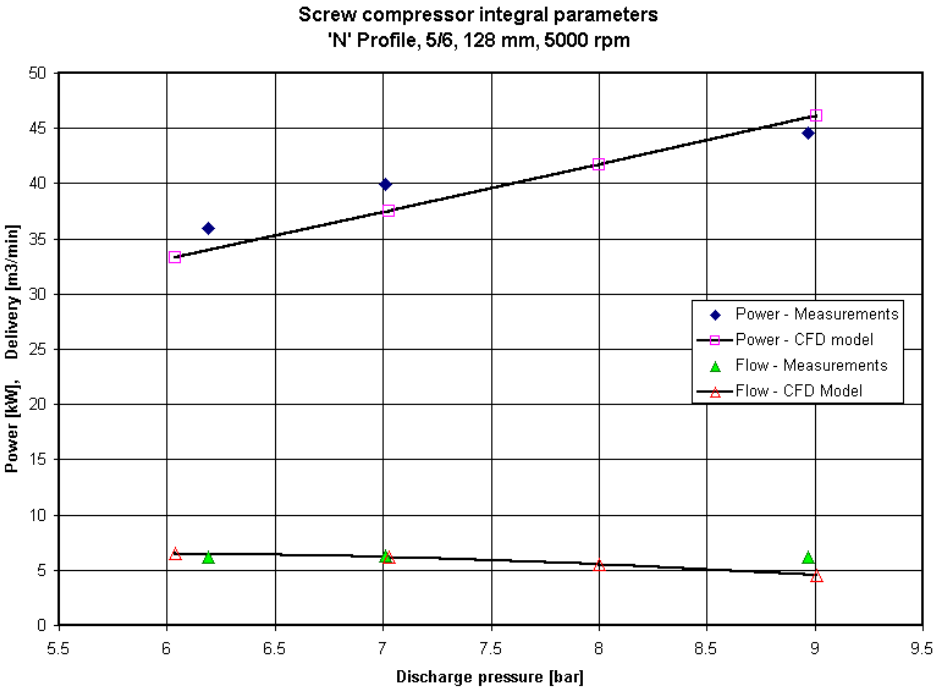

Figure 14 Comparison of the integral parameters at 5000 rpm shaft speed